Spatial Estimates of Stormwater-Pollutant Loading Using Bayesian Networks and Geographic Information Systems

Mi-Hyun Park, Michael K. Stenstrom

ABSTRACT: Stormwater runoff has become the primary source of many pollutants to the Santa Monica Bay watershed (California), and managing stormwater inputs to the bay has become the primary objective of new regulatory efforts. Empirical methods to estimate stormwater pollution have been developed using land-use data; however, land-use data collected from traditional ground surveys are expensive and time consuming and may not be available. This study used an alternative approach and estimated land use from satellite-image classification using Bayesian networks. The results were converted to thematic maps using a geographic information system to visualize spatial estimates of runoff coefficients of the given area, event-mean concentrations (EMCs) of target pollutants, and their pollutant loads. The stormwater-pollutant-loading maps identified areas of high annual-mass loads, which were more affected by impervious areas, because of their high runoff coefficients, rather than their EMCs. In this watershed, the major sources of nonpoint-source pollution are the multiple-family-residential (14%), commercial (7%), public (6%), industrial (3%), and transportation (7%) land uses adjacent to Marina del Rey and the Ballona wetlands. The contributions of single-family-residential (30%) and open (33%) land uses are less important. *Water Environ. Res.,* **78,** 421 (2006).

KEYWORDS: stormwater-runoff pollution, satellite-image classification, geographic information system, Bayesian networks.

doi:10.2175/106143006X98813

Introduction

Stormwater runoff has received increasing attention in the Santa Monica Bay watershed to protect its surface-water quality because most point-source pollution has been treated to reduce its effect on receiving waters (Ackerman and Schiff, 2003; Bay et al., 1999 and 2003). Much of the Santa Monica Bay watershed has been developed as a result of rapid population growth, and the urbanization is still ongoing, especially in the areas surrounding Ballona wetlands. Urban-stormwater-runoff pollution is known to be related to land-use activities (Perry and Vanderklein, 1996; Sliva and Williams, 2001); therefore, urban-land-use information is important in managing stormwater-runoff pollution.

Monitoring stormwater runoff and predicting pollutant loading to receiving waters from monitoring results are not easy tasks, because these demand expertise and accumulated data (Duncan, 1995; Vaze and Chiew, 2003). Modeling loads from land-use and rainfall data is an alternative approach (Chiew and McMahon, 1999; Stenstrom et al., 1984), but conventional land-use data collection methods, such as ground surveys, can also be time-consuming and resource-intensive. Vaze and Chiew (2003) have reviewed monitoring and modeling efforts for stormwater quality, and few attempts have been made to spatially estimate the pollutant loading in an inexpensive and consistent way. This research proposes the use of satellite imagery to estimate stormwater-pollutant loading in a typical urban area. Satellite imagery can provide repetitive and inexpensive information and have been extensively used for environment monitoring (Haack et al., 1987; Park and Stenstrom, 2003; Ridd and Liu, 1998; Stefanov et al., 2001).

We used Bayesian networks to classify the satellite imagery. Bayesian networks are an artificial intelligence tool and have been successfully used in many applications, including environmental areas (Borsuk et al., 2004; Sahely and Bagley, 2001; Varis, 1998). Bayesian networks provide both probabilistic expression and graphical representation. As probabilistic expression, Bayesian networks are based on Bayes' theorem, so that the posterior probability of a target variable can be calculated from prior probability and likelihoods.

Figure 1 shows a simplified Bayesian network example of a water-quality problem. There is one variable associated with the hypothesis "is the water safe? (W)", and three measured variables, "turbidity (T), odor (O), and color (C)". Bayes' theorem requires that the variables be conditionally independent given W, which means that if W is known, the value of T does not add any additional information about O or C, and vice-versa. Given conditional independence and the probability distributions summing to 1, then the following equation represents Bayes' theorem:

$$P(W|T, O, C) = \alpha P(T|W)P(O|W)P(C|W)P(W) \tag{1}$$

Where

α = a parameter adjusted to normalize the probabilities to 1.
$P(W)$ = the prior probability of the water safety, which can be determined from water-quality records and other subjective information.

If the records for T, O, C given W are known, then the likelihood of $P(T|W)$, $P(O|W)$ and $P(C|W)$ can be computed from data. Equation 1 can be used to calculate posterior probability distribution over W given T, O, and C.

As the graphical representation of the Bayesian network describing water quality, Figure 1 is a directed-acyclic graph, with nodes and arcs (Pearl, 1988). In the network, each node corresponds to a variable, and a pair of dependent nodes is connected with a directed arc without creating a loop. Therefore, the structure of the network

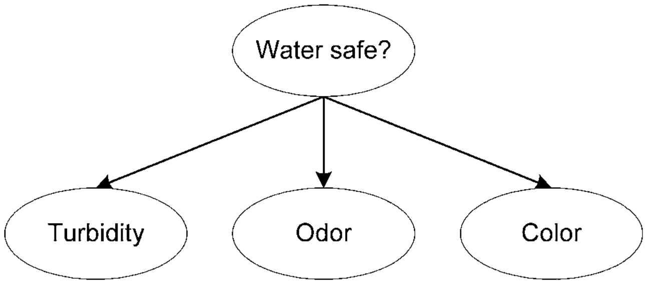

Figure 1—An example of a Bayesian network.

explicitly shows the dependency relationships among nodes, and the dependency between nodes is quantified using a conditional-probability table. This makes the dependency relationship easily understood in the given domain. Figure 1 explicitly shows that water safety is dependent on turbidity, odor, and color of the water. In this case, the hypothetical node, "water safe?" is called *class node* and other measured nodes are its *child nodes.*

Bayesian networks offer other benefits in that they can adopt subjective information from experts and objective information from data (Heckerman, 1995). For example, if the historical records of water safety are not known, they could be inferred from the opinions of experts. The networks are flexible and can incorporate additional information to an existing network when updating. The output can be viewed as either values or probabilities of each (Russell and Norvig, 1995). Also, Bayesian networks can handle problems with uncertainties, such as missing data (Heckerman, 1995). Bayesian networks are able to provide a higher level of explanation by identifying those nodes that are most important in reaching the conclusion (Ripley, 1996).

The main objective of this research is to generate spatial estimates of pollutant loads. This is necessary because the magnitudes and ratios of pollutant loads can be inferred from the runoff and event-mean concentrations (EMCs) data, but cannot be spatially identified. To accomplish this objective, we conducted Bayesian-network classification of urban-land use from satellite imagery. The urban-land-use information provides the runoff coefficients and EMCs for each pollutant, which are necessary for calculating pollutant loads. Pollutant loading maps using geographic information systems (GIS) were generated, which identify the areas that discharge the highest pollutant loadings. The value of the spatial estimates is used, not only to determine the high loading areas, but also to locate and visualize them so that planners can better develop best-management practices (BMPs). The classification of land uses that produce similar loadings can be combined, which should simplify stormwater management.

Materials and Methods

Study Area and Data. Santa Monica Bay provides recreational resources and important ecological resources for natural habitat (Dojiri et al., 2003). One of the few natural habitats in the Santa Monica Bay watershed is the Ballona wetlands, which are the only wetlands in west Los Angeles. The Ballona wetlands are important to protect Santa Monica Bay in that they buffer the effects of stormwater runoff from the surrounding urban areas (Ballona Wetlands Land Trust, 2005). The wetlands have been degraded over the past 50 years by continuing urbanization and excessive intrusion of fresh water (Ballona Wetlands Foundation, 2005).

The study area was Marina del Rey, which includes the Ballona wetlands and their adjacent areas in the Santa Monica Bay watershed, as shown in Figure 2. This area has a moderate climate, with an average annual rainfall of 360 mm (National Oceanic and Atmospheric Administration, 2005), which occurs mainly during winter. The size of the area is 22 km^2 and contains different urban features. The study area predominantly consists of residential and open areas, and urbanization is still continuing.

We used a Landsat Extended Thematic Mapper Plus (ETM^+) image (National Aeronautics and Space Administration, Greenbelt, Maryland; NASA, 2002), which was obtained on August 11, 2002, with path 41 and row 36 covering the study area. The ETM^+ sensor provides eight band images: bands 1, 2, and 3 are visible bands of blue, green, and red, respectively; band 4 is near infrared; bands 5 and 7 are middle infrareds; band 6 is thermal infrared; and band 8 is panchromatic. The spectral signals of all bands are recorded in 8 bits, with digital numbers between 0 (black) and 255 (white). The image has spatial resolution of the image of 30 meters for all bands, except the thermal infrared and panchromatic bands, which have spatial resolutions of 60 and 15 meters, respectively. Table 1 summarizes the characteristics of the Landsat ETM^+ system. In this study, we clipped a sub-image of the study area from all bands, except the panchromatic band. Water in the sub-image was masked and not

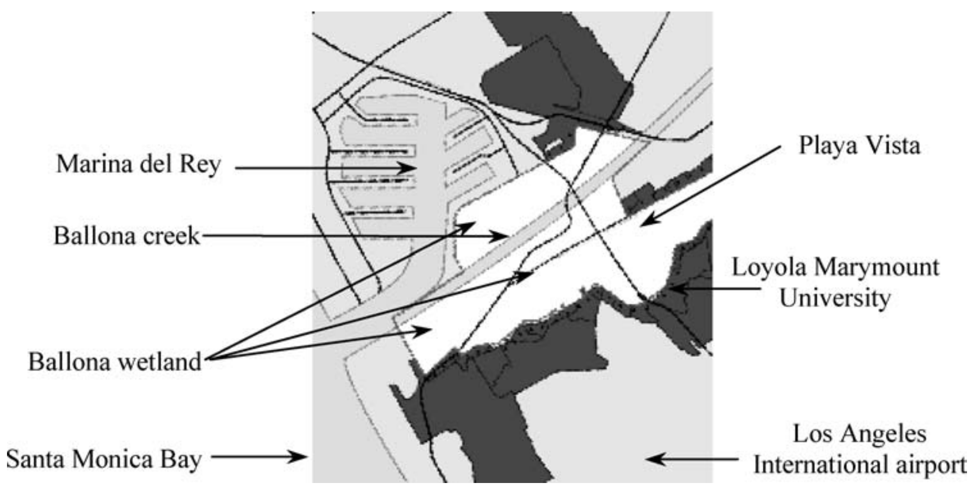

Figure 2—Study area of Ballona Creek watershed and its vicinity.

Table 1—Summary of Landsat ETM+ system.*

Band	Spectral resolution	Spatial resolution	Temporal resolution	Radiometric resolution
1 (blue)	0.45 to 0.52 μm			
2 (green)	0.52 to 0.60 μm			
3 (red)	0.63 to 0.69 μm	30 × 30 m		
4 (near IR)	0.76 to 0.90 μm			
5 (IR)	1.55 to 1.75 μm		16 days	8 bits
6 (thermal IR)	10.4 to 12.5 μm	60 × 60 m		
7 (IR)	2.08 to 2.35 μm	30 × 30 m		
8 (panchromatic)	0.52 to 0.90 μm	15 × 15 m		

* (after Jensen, 2000).

Table 2—Summary of land-use pixels for training and test data.

Land-use class	Training data	Test data	Ratio
Single-family residential	547	273	26%
Multiple-family residential	240	120	12%
Commercial	143	72	7%
Public	133	67	6%
Industrial	123	62	6%
Transportation	197	98	9%
Open	684	341	33%
Total	2067	1033	100%

considered because land-use only is of interest in this study. The input data also included geospatial information as ancillary data (the X and Y coordinate values of each pixel).

For training data and test data for accuracy assessment, we used three different ground-reference-data sets: land-use data from the Southern California Association of Governments (SCAG, 2003), aerial photos, and field-survey information. Both training data and test data were collected from all classes in proportion to their abundance in the entire data set. The total number of pixels for training data and test data was 2067 and 1033, which corresponded to 8.5 and 4.3% of total data, respectively. The detailed information of training data and test data is given in Table 2.

Land-Use Classification. All data values were discretized because Bayesian networks mostly deal with discrete values. For example, all spectral band and ancillary data were discretized to 15 values, based on equal frequency interval. The class node had seven states corresponding to modified U.S. Geological Survey (USGS) level III land uses (Anderson et al., 1976): single-family-residential, multiple-family-residential, commercial, public, light-industrial, transportation, and open land-use area.

Tree-structured Bayesian networks were developed for classification by selecting land use as the class node. The networks were constructed from data based on mutual information between nodes because mutual information provides dependency information (Chow and Liu, 1968).

$$\mathrm{MI}(v_i, v_j) = \sum_{v_i \times v_j} P(v_i, v_j) \log\left[\frac{P(v_i, v_j)}{P(v_i)P(v_j)}\right] \tag{2}$$

Where

$\mathrm{MI}(v_i,v_j)$ = mutual information of random variables of v_i and v_j.
$P(v_i,v_j)$ = a joint probability of v_i and v_j, and
$P(v_i)$ and $P(v_j)$ = the probabilities of each random variable.

Mutual information is zero for completely independent variables, but increases with dependence between variables.

For evaluating the network performance, the overall accuracy and confusion matrix were used (Foody, 2002). Overall accuracy alone cannot provide individual class accuracy, and, therefore, individual class errors from the confusion matrix were calculated. A confusion matrix is a table of the resulting map-class labels (i.e., single-family residential) as rows compared with the known-class labels as columns. The matrix elements show the number of pixels identified under the class label. From the confusion matrix, two types of errors can be identified: omission and commission. Omission error provides a measure of the pixels actually belonging to a class, but failed to be assigned to the class, and commission error provides a measure of the pixels that are incorrectly assigned to the class, but actually belong to other classes.

$$\text{Omission error} = 1 - \frac{N}{\sum N_c} \tag{3}$$

$$\text{Commission error} = 1 - \frac{N}{\sum N_r} \tag{4}$$

Where

N = number of pixels correctly classified (shown as the diagonal of the confusion matrix),
$\sum N_c$ = total number of pixels in the original class of interest, and
$\sum N_r$ = total number of pixels assigned to the class.

Spatial Estimates. Empirical models have been developed for stormwater runoff and pollutant loading, based on land-use data (Ackerman and Schiff, 2003; Stenstrom and Strecker, 1993; Wong et al., 1997). The *runoff coefficient*, defined as the average ratio of runoff to rainfall (Wong et al., 1997), is the fraction of rainfall that actually reaches the receiving water. The runoff coefficient is highly correlated to imperviousness of the area. The following equation (Driscoll et al., 1990) is an example of this relationship:

$$\mathrm{RC} = 0.7 \times \mathrm{I} + 0.1 \tag{5}$$

Where

RC = the runoff coefficient (dimensionless), and
I = the impervious fraction (dimensionless).

The runoff coefficient is the main component to determine annual-average-storm-runoff volume. The annual-average storm-runoff volume, based on the rational method (Viessman and Knapp, 1989; Wong et al., 1997), can be calculated as follows:

$$\mathrm{RV} = \mathrm{RC} \times \mathrm{A} \times \mathrm{CF} \times \mathrm{RF} \tag{6}$$

Where

RV = annual-average-storm-runoff volume (m^3),
A = drainage area (m^2),
CF = conversion factor ($m/10^3 mm$), and
RF = average storm rainfall (mm).

If we multiply RV with the number of storms in the given year, we can get the annual-average-storm runoff, as follows:

Table 3—Runoff coefficient (RC) and water-quality characteristics (EMCs) based on urban-land use in Santa Monica Bay watershed.*

Land use	Runoff coefficient	Total suspended solid (mg/L)	Chemical-oxygen demand (mg/L)	Total Kjeldahl nitrogen (mg/L)	Total phosphorus (mg/L)	Total copper (mg/L)	Lead (mg/L)	Zinc (mg/L)	Oil and grease (mg/L)
Single residential	0.39	290	140	4.3	0.85	0.095	0.350	0.350	3
Multiple residential	0.58	210	130	2.4	0.62	0.100	0.440	0.380	22
Commercial	0.74	180	90	2.0	0.43	0.072	0.225	0.694	22
Public	0.66	180	90	2.0	0.43	0.072	0.225	0.694	22
Industrial	0.74	180	90	2.0	0.43	0.072	0.225	0.694	22
Transportation	0.66	210	130	2.4	0.62	0.100	0.440	0.380	22
Open	0.1	490	95	2.8	0.52	0.055	0.140	0.440	0

* (after Stenstrom and Strecker, 1993).

$$RV_a = RV \times N_{storm} \tag{7}$$

Where

RV_a = annual-average-storm runoff (m^3/y), and
N_{storm} = average number of storms per year (y^{-1}).

If we have information of EMCs for each water-quality parameter, we can obtain annual pollutant loading from the following equation:

$$PL_i = RV_a \times EMC_i \tag{8}$$

Where

PL_i (kg/y) = annual pollutant loading, and
EMC_i (mg/L) = EMCs for water-quality parameter, i.

Runoff coefficients and EMCs of each water-quality parameter, based on different land uses in Santa Monica Bay watershed, are shown in Table 3. If we assume that the rainfall and annual number of storms are equal for all pixels and all stormwater-runoff discharges to Santa Monica Bay, the following equation represents pollutant loads per unit pixel and unit rainfall:

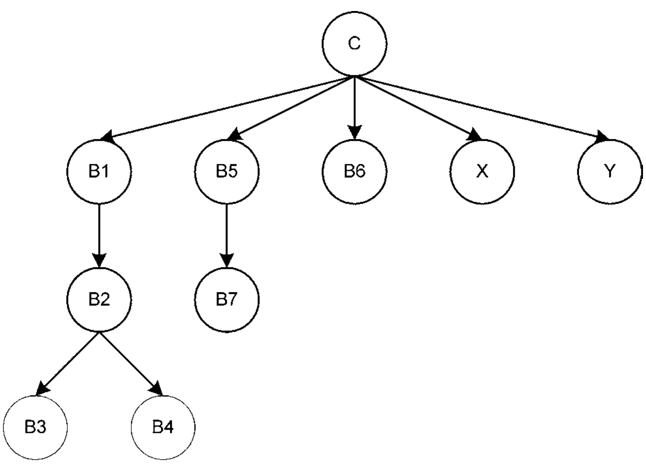

Figure 3—The structure of Bayesian networks for urban land use classification Note that C is the class node representing urban land use, B1 to B7 represent digital numbers of Landsat ETM$^+$ band 1 to 7 of a pixel, X is x-coordinate value of a pixel and Y is y-coordinate value of a pixel.

$$PL_i = \alpha \times RC \times EMC_i \tag{9}$$

Where

α = a normalization factor that depends on units and conversion factors.

These equations were adopted to generate thematic maps from land-use information.

ArcGIS version 8.3 (ESRI, Redlands, California) was used for GIS implementation. The land-use map was developed first from the database of land-use-classification results. The resulting land-use map was converted to maps of delineated impervious surfaces with runoff coefficients, EMCs, and pollutant loadings. In each case, land-use pixel is the unit of analysis. Eight water-quality parameters were examined: chemical oxygen demand (COD), total suspended solids (TSS), nutrients (i.e., total Kjeldahl nitrogen [TKN] and total phosphorus [TP]), total copper (Cu), total lead (Pb), total zinc (Zn), and oil and grease (O&G). The EMCs and pollutant loading had three states: low, medium, and high. Each state of a particular water-quality parameter corresponded to the land use based on eq 9.

Results

The structure of Bayesian networks is shown in Figure 3. The network structure shows the dependency among variables. For example, bands 1, 2, and 3 are connected, which are often highly correlated (Mather, 1999) because they are all visible bands. In the same way, bands 5 and 7 are also dependent, and both are middle infrared bands. Moreover, the structure shows that bands 1, 5, and 6 are the most contributing input variable to determine the value of the class node among the spectral inputs. Geospatial ancillary data were

Table 4—Errors of the each land use (%).

Land use	Omission error	Commission error
Single-family residential	14.9	8.1
Multiple-family residential	28.9	32.5
Commercial	42.4	47.2
Public	42.9	64.2
Industrial	28.4	22.6
Transportation	17.9	20.4
Open	9.3	5.9

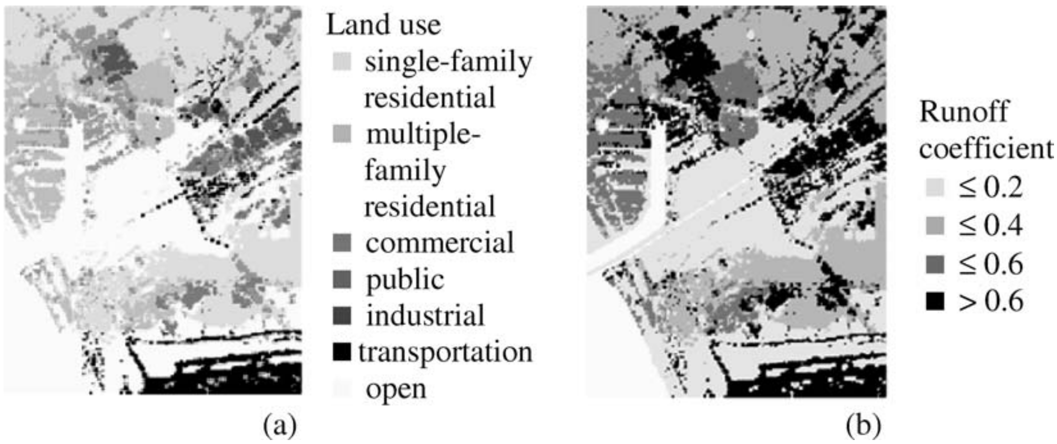

Figure 4—Maps of the Ballona Wetlands and vicinity including spectral data and geospatial data (a) land use classification and (b) impervious surfaces associated with runoff coefficient.

also important inputs to correctly predict the land use of each pixel. The overall accuracy of land-use classification was 81%. The omission and commission errors are given in Table 4, which shows that Bayesian networks predicted open, single-family-residential and transportation land uses with errors less than 20%. Commercial and public land uses were not well-assigned compared to other land uses, and they were often mistaken with each other and industrial land use.

Figure 4 shows maps of land use and the impervious surfaces associated with runoff coefficients in the study area. Impervious surfaces were classified into four states, which were converted from the land-use map. Open-land use, corresponding to the area with the lowest runoff coefficient of 0.1, was converted to pervious area (runoff coefficient $\leq$ 0.2). Single-family-residential-land use was converted to the low impervious area, with a runoff coefficient of

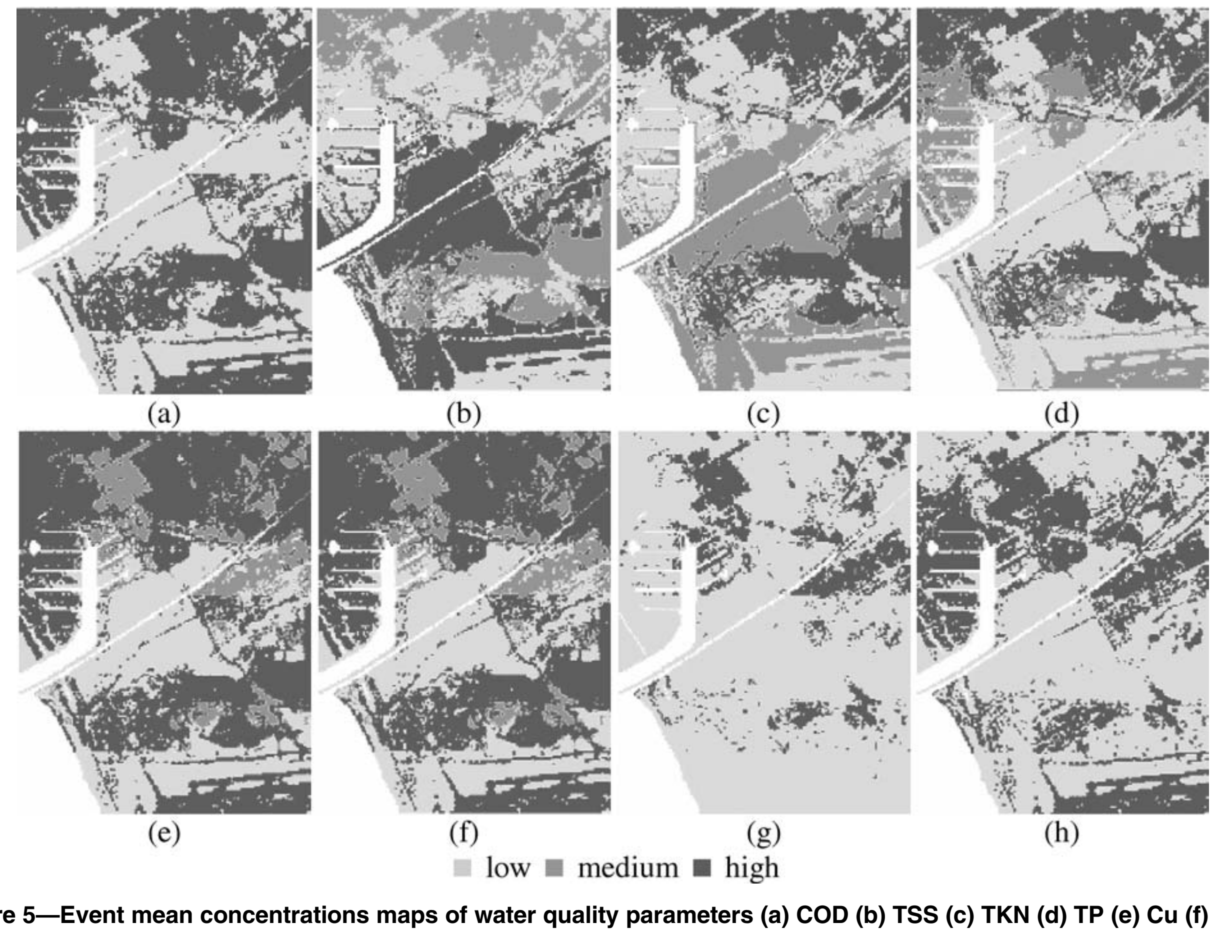

Figure 5—Event mean concentrations maps of water quality parameters (a) COD (b) TSS (c) TKN (d) TP (e) Cu (f) Pb (g) Zn (h) oil and grease.

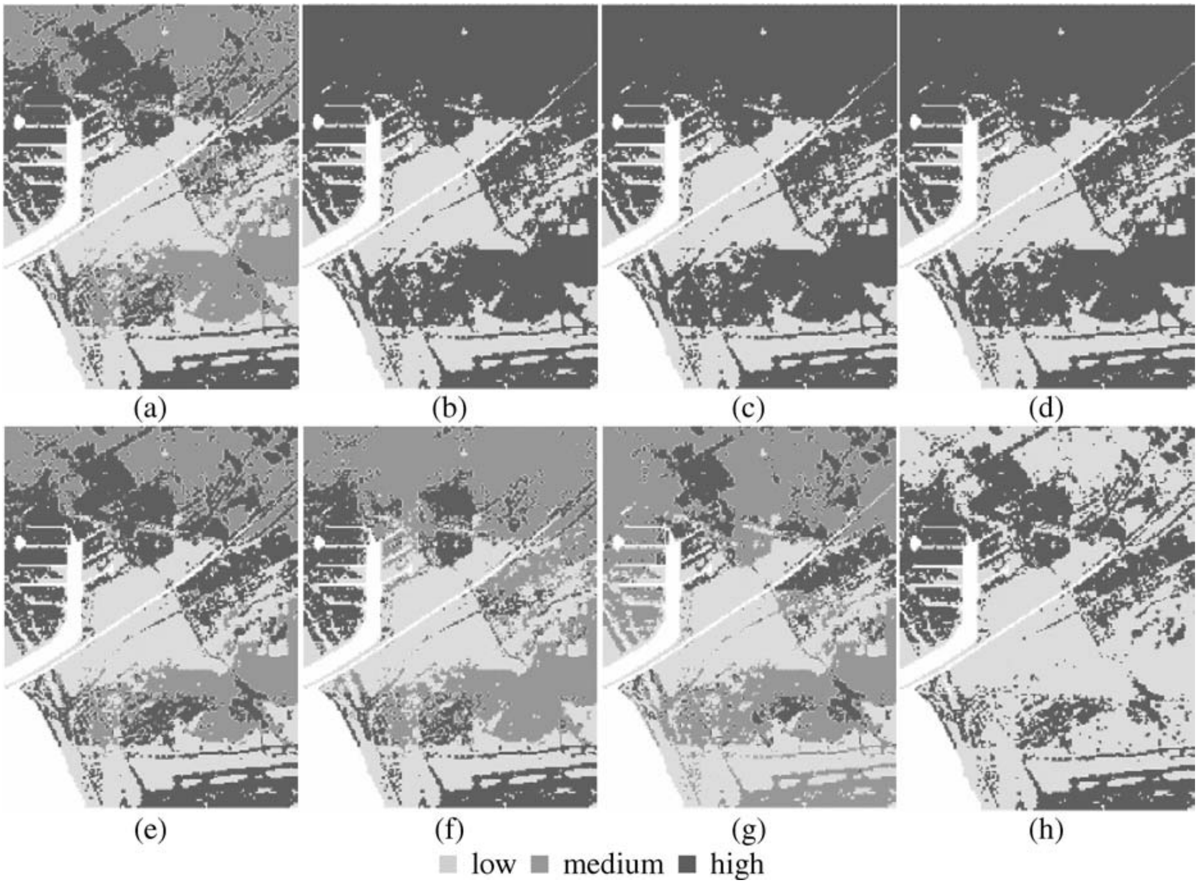

Figure 6—Pollutant loading maps of water quality parameters (a) COD (b) TSS (c) TKN (d) TP (e) Cu (f) Pb (g) Zn (h) oil and grease.

0.4, and multiple-family- residential-land use to the medium impervious area (runoff coefficient $\leq$ 0.6). The rest of land uses corresponded to the highly impervious areas (runoff coefficient $>$ 0.6).

Figure 5 shows EMC maps for each water-quality parameter in the study area to see which areas are the major sources generating stormwater pollution. We should stress that the EMCs in the Santa Monica Bay watershed tend to be higher than those reported in the U.S. Environmental Protection Agency's Nationwide Urban Runoff Program (NURP) database (Driscoll et al., 1990; Wong et al., 1997). All EMC maps were converted from the land-use map based on the relationships, as shown in Table 3. The EMCs were generally classified into three states: low, medium, and high; however, COD, Zn, and O&G maps displayed only two states. Residential- and transportation-land uses tended to increase the COD EMC, while the rest of land uses tended to lower the EMC. Open-land use tended to increase the TSS EMC, while other land uses, except single-family-residential, tended to lower the TSS EMC. Single-family-residential-land use was the most significant contributor of nutrients. The EMC maps of Cu and Pb were identical in that residential- and transportation-land uses were responsible for high EMC, and open-land use corresponded to low EMC areas. The EMC map of Zn exhibited different behavior than other water-quality parameters: commercial, public, and industrial land uses showed high EMC and residential-, transportation-, and open-land uses showed low EMC. The sources of Zn, Cu, and Pb are different, and there are many sources of Zn, including atmospheric deposition, automobile tires, paint, and roofing materials (Davis et al., 2001; Förster, 1999; Kszos et al., 2004; Lu et al., 2003; Schiff and Stolzenbach, 2003), which may explain their different behavior. The high EMC of O&G is mainly caused by multiple-residential, commercial, public, industrial, and transportation land uses, and contribution of the other two land uses was trivial.

Figure 6 shows pollutant-loading maps for each water-quality parameter, which is proportional to the product of the runoff coefficient and EMC. Pollutant loads were also classified into three states, but TSS, TKN, TP, and O&G cases had only two states, and the medium state was not represented in the final result. High COD emissions were generated from multiple-family-residential, commercial, industrial, and transportation land uses. Single-family-residential and public-land uses corresponded to medium load, and open-land use corresponded to low load. The pollutant-loading maps of TSS, TKN, and TP were identical because all land uses, except open-area land use, significantly contributed to high load. The Cu map shows that single-family-residential-land use corresponded to medium load, open-land use to low load, and all the other land uses to high load. For the Pb, the high load mainly came from multiple-family-residential and transportation land uses. Open-land use also generated low load, and the other four land uses created medium load. The Zn case shows low loads from open land use, medium loads from residential and transportation land uses, and high loads from commercial, public, and industrial land uses. Multiple-family-residential, commercial, public, industrial, and transportation land uses created high O&G loads, whereas single-family-residential and open land uses produced low loads. The O&G pollutant loadings were identical to the EMC maps, which was not true for the other pollutants. The reason is the large relative change in O&G EMCs (0 to 22 mg/L) as compared to the smaller relative change for other pollutants, such as COD (90 to 140 mg/L).

Figure 7 compares the pollutant loading and EMCs as a percentage of total area. The percentage of areas corresponding to the high, medium, and low categories are compared. The result shows that the pollutant loading did not necessarily correspond to the EMCs. The differences were a result of the varying imperviousness or runoff coefficient, which will be discussed later. Over 65% of the area generated high pollutant loads for TSS, TKN, and TP. Only 15% of the area generated high Zn loadings, and only 22% of the area generated high Pb loading. Open areas tended to reduce pollutant loadings, and 33% of the areas were classified as low because of the contribution of the open-area land use, for all pollutants except O&G.

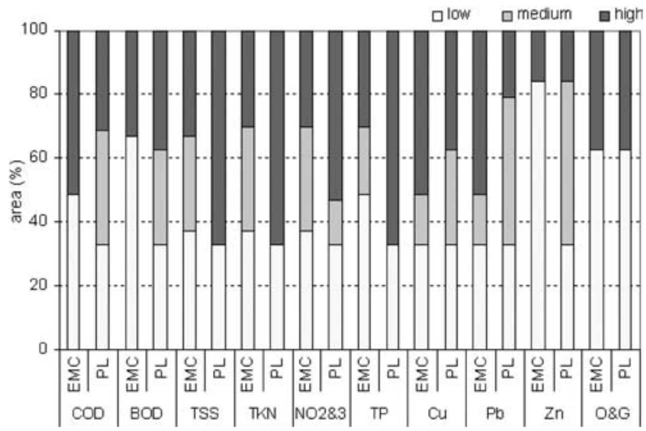

Figure 7—Comparison of areas of EMC and pollutant loading for each water quality parameter.

Discussion

Using satellite imagery for land-use classification is an effective alternative to the conventional ground-surveyed land use. Estimating land use from satellite imagery reduces time to collect the information. Sleavin et al. (2000) reported that satellite imagery reduces cost and time, especially in large areas, because ground surveys require extensive fieldwork. Using satellite imagery can avoid possible errors in ground-surveyed land use. For example, the vegetation areas inside the Los Angeles International Airport (California) were assigned to open-land use instead of transportation as in SCAG land use. Vegetated areas and parking lots in Loyola Marymount University (Los Angeles, California) were assigned to open- and transportation-land uses respectively, which both belonged to public in the SCAG land-use data. The areas under construction in Playa Vista (west Los Angeles, California [see Figure 2]) showed transportation- and industrial-land uses, depending on the degree of construction. Satellite-image classification captured the boats at anchor in Marina del Rey, which are not present in the ground-surveyed land use. The errors in the ground-surveyed-land-use maps may result because the purpose of the survey is generally for non-environmental objectives, such as urban planning or tax collection. Adjacent areas of differing environmental importance may be merged because they are not different with respect to urban planning or tax collection. In addition, satellite imagery can be applicable to those areas where land-use data are not readily available.

Some urban-land uses in the satellite image exhibit similar spectral signatures and are not easily distinguished (Richards and Jia, 1999; Stefanov et al., 2001). Commercial- and public-land uses were often misclassified, and their omission and commission errors were more than 40%. Public- and commercial-land uses may have similar spectral signatures, because classification of commercial- and public-land use often differs by the ownership of the similar activities. For example, publicly owned buildings may be similar to privately owned buildings when viewed by satellite. Fortunately, misclassification of commercial- and public-land uses does not significantly affect the spatial estimates of pollutant loading because they often generate similar pollutant loads.

The pollutant-loading maps show that the lowest loading areas primarily correspond to open-area land use, which exhibit a low runoff coefficient. The highest pollutant loading areas of TSS, TKN, TP, Cu, and O&G correspond to the areas with a high runoff coefficient, i.e., commercial, public, industrial, and transportation land uses. Even for the other water-quality parameters, those land uses with a high runoff coefficient corresponded to at least medium or high pollutant-loading areas. Therefore, it is important to identify areas with a high runoff coefficient to properly manage stormwater-pollutant loads. This is logical conclusion because stormwater may be retained by vegetation or infiltrated through the pervious ground, whereas stormwater overland runoff is conveyed into receiving water through impervious surfaces. Highly impervious surfaces should be avoided, when possible, to reduce runoff volume.

The comparison between the EMC map and the loading map of each pollutant type shows that high EMC generating areas do not always match high-pollutant-loading areas. For example, areas with high TSS EMC correspond to low TSS loading because of the very low runoff coefficient associated with open-land use. Furthermore, for COD, TSS, TKN, and TP, low EMC areas correspond to high loading areas. This occurs because the ratio of high EMCs to low EMCs ranges from 1.6 to 2.7, while the ratio of high to low runoff coefficients is 7.4. The result shows that low-EMC-generating areas should not be underestimated or ignored for their potential effect on the receiving water quality. These differences translate into higher ranges of pollutant loads.

Conclusions

This paper has shown that satellite-image classification is useful in estimating stormwater-pollutant loads. The methodology used here has advantages over conventional approaches based on ground surveys because of its applicability to areas where land-use data are not available, such as in developing countries. Moreover, using satellite images can provide information that is optimized for environmental purposes.

Bayesian-network classification is useful in that the approach reduces the dimension of inputs for classification by identifying the most informative input variables to classification. Bayesian networks provide fast computation with reasonable accuracy, despite the mixed characteristic of urban-land uses. The potential error of commercial- and public-land uses can be easily resolved because they can be included in the same class when generating a pollutant-loading map. The Bayesian technique also identified and classified areas that are chronically misclassified, providing more accurate estimates.

The pollutant-loading maps can assist in developing best-management strategies by identifying areas of high pollutant loading. In this case study, areas neighboring the Ballona wetlands and, particularly, in the western part of Marina del Rey are the high-emitting areas. The continuing urbanization of Playa Vista would increase the pollutant loads to Santa Monica Bay, without the proposed BMPs.

The pollutant-loading maps show that the loadings were more affected by the runoff coefficient than EMC for most of the land uses. This results because there is more variation in runoff coefficient than EMC among the land uses. Therefore, elimination or reduction of impervious surfaces may be more important than BMPs that reduce the EMCs by partial treatment. Multiple-family-residential, commercial, industrial, and transportation land uses contribute proportionally more, especially for COD, TSS, TKN, and TP. These land uses should be targeted for the first application of BMPs.

Acknowledgments

Credits. This work was partially supported by the U.S. Environmental Protection Agency under grant R825831.

Authors. Mi-Hyun Park is a doctoral student and Michael. K. Stenstrom is a professor in Department of Civil and Environmental Engineering at the University of California, Los Angeles. Correspondence should be addressed to Mi-Hyun Park, Dept. of Civil and Environmental Engineering, University of California, Los Angeles, 5714 Boelter Hall, Los Angeles, CA, 90095, email: mhpark@seas.ucla.edu

Submitted for publication June 14, 2004; revised manuscript submitted January 18, 2005; accepted for publication February 22, 2005.

The deadline to submit Discussions of this paper is July 15, 2006.

References

Ackerman, D.; Schiff, K. (2003) Modeling Storm Water Mass Emissions to the Southern California Bight. *J. Environ. Eng. ASCE,* **129** (4), 308–317.

Anderson, J. R.; Hardy, E.; Roach, J.; Witmer, R. (1976) A Land-Use and Land-Cover Classification System for use with Remote Sensor Data; U.S. Geological Survey Profession paper 964; U.S. Geological Survey: Reston, Virginia.

Ballona Wetlands Foundation (2005) http://www.ballona-wetlands.org/pages/factsa.html; Ballona Wetlands Foundation: Los Angeles, California.

Ballona Wetlands Land Trust (2005) http://www.ballona.org/f-important.asp; Ballona Wetlands Land Trust: Playa del Ray, California.

Bay, S.; Jones, B. H.; Schiff, K. (1999) Study of the Impact of Stormwater Discharge on the Beneficial Uses of Santa Monica Bay; Executive Summary Prepared for Los Angeles County Department of Public Works: Alhambra, California.

Bay, S.; Jones, B. H.; Schiff, K.; Washburn, L. (2003) Water Quality Impacts of Stormwater Discharges to Santa Monica Bay. *Marine Environ. Res.,* **56,** 205–223.

Borsuk, M. E.; Stow, C. A.; Reckhow, K. H. (2004) A Bayesian Network of Eutrophication Models for Synthesis, Prediction, and Uncertainty Analysis. *Ecol. Model.,* **173,** 219–239.

Chiew, F. H. S.; McMahon, T. A. (1999) Modelling Runoff and Diffuse Pollution Loads in Urban Areas. *Water Sci. Technol.,* **39** (12), 241–248.

Chow, C. K.; Liu, C. N. (1968) Approximating Discrete Probability Distributions with Dependence Trees. *IEEE Trans.Inform. Theory,* **IT-14** (3), 462–467.

Davis, A. P.; Shokouhian, M.; Ni, S. (2001) Loading Estimates of Lead, Copper, Cadmium, and Zinc in Urban Runoff from Specific Sources. *Chemosphere,* **44,** 997–1009.

Dojiri, M.; Yamaguchi, M.; Weisberg, S. B.; Lee, H. J. (2003) Changing Anthropogenic Influence on the Santa Monica Bay Watershed. *Marine Environ. Res.,* **56,** 1–14.

Driscoll, E. D.; Shelly, P. E.; Strecker, E. W. (1990) *Pollutant Loadings and Impacts from Stormwater Runoff*, Volume III: Analytical Investigation and Research Report, FHWA-RD-88-008, Federal Highway Administration: Washington, D.C.

Duncan, H. P. (1995) A Review of Urban Stormwater Quality Processes; Report No. 95/9, Cooperative Research Centre for Catchment Hydrology: Melbourne, Australia.

Foody, G. M. (2002) Status of Land Cover Classification Accuracy Assessment. *Remote Sensing Environ.,* **80** (1), 185–201.

Förster, J. (1999) Variability of Roof Runoff Quality. *Water Sci. Technol.,* **39** (5), 137–144.

Haack, B.; Bryant, N.; Adams, S. (1987) An Assessment of Landsat MSS and TM Data for Urban and Near-Urban Land-Cover Digital Classification. *Remote Sensing Environ.,* **21,** 201–213.

Heckerman, D. (1995) A Tutorial on Learning with Bayesian Networks; Technical Report MSR-TR-95-06, Microsoft Research: Redmond, Washington.

Jensen, J. R. (2000) *Remote Sensing of the Environment: An Earth Resource Perspective.* Prentice Hall: Upper Saddle River, New Jersey.

Kszos, L. A.; Morris, G. W.; Konetsky, B. K. (2004) Source of Toxicity in Storm Water: Zinc from Commonly Used Paint. *Environ. Toxicol. Chem.,* **23** (1), 12–16.

Lu, R.; Turco, R. P.; Stolzenbach, K.; Friedlander, S. K.; Xiong, C.; Schiff, K.; Tiefenthaler. L.; Wang, G. Y. (2003) Dry Deposition of Airborne Trace Metals on the Los Angeles Basin and Adjacent Coastal Waters. *J. Geophys. Res. Atmosph.,* **108** (D2), 4074.

Mather, P. M. (1999) *Computer Processing of Remotely-Sensed Images: An Introduction*, Wiley: Chichester, United Kingdom.

NASA (2002) http://landsat.gsfc.nasa.gov/announcements/landsat7.pdf; National Aeronautics and Space Administration: Washington, D.C.

National Oceanic and Atmospheric Administration (2005) Los Angeles/Oxnard; http://www.nwsla.noaa.gov/climate/cvc.html; National Oceanic and Atmospheric Administration: Washington, D.C.

Park, M.; Stenstrom, M. K. (2003) Land Use Classification for Stormwater Modeling Using Bayesian Networks. In *Proceedings of the 7th International Specialised IWA Conference, Diffuse Pollution and Basin Management*, Dublin, Ireland, August 17–22; International Water Association, London, United Kingdom.

Pearl, J. (1988) *Probabilistic Reasoning in Intelligent Systems: Networks of Plausible Inference.* Morgan Kaufmann: San Mateo, California.

Perry, J.; Vanderklein, E. (1996) *Water Quality Management of a Natural Resource.* Blackwell Science: Cambridge, Massachusetts.

Richards, J. A.; Jia, X. (1999) *Remote Sensing Digital Image Analysis: An Introduction.* Springer: Heidelberg, Germany.

Ridd, M. K.; Liu, J. (1998) A Comparison of Four Algorithms for Change Detection in an Urban Environment. *Remote Sensing Environ.,* **63,** 95–100.

Ripley, B. D. (1996) *Pattern Recognition and Neural Networks.* University Press: New York.

Russell, S.; Norvig, P. (1995) *Artificial Intelligence: A Modern Approach.* Prentice Hall: Upper Saddle River, New Jersey.

Sahely, B. S. G. E.; Bagley, D. M. (2001) Diagnosing Upsets in Anaerobic Wastewater Treatment Using Bayesian Belief Networks. *J. Environ. Eng. ASCE,* **127** (4), 302–310.

Schiff, K.; Stolzenbach, K. (2003) Contribution of Trace Metals via Atmospheric Deposition to Santa Monica Bay and the Santa Monica Bay Watershed. *Proceedings of Water Environment Federation Total Maximum Daily Load 2003 Conference Proceedings*, Chicago, Ilinois, November 16–19; Water Environment Federation: Alexandria, Virginia.

Sliva, L.; Williams, D. D. (2001) Buffer Zone Versus Whole Catchment Approaches to Studying Land Use Impact on River Water Quality. *Water Res.,* **35** (14) 3462–3472.

Southern California Association of Governments (2003) http://wagsdata.scag.ca.gov; 818 W. Seventh Street, 12th Floor (Main Office) Los Angeles, CA 90017.

Sleavin, W.; Civco, D. L.; Prisloe, S.; Giannotti, L. (2000) Measuring Impervious Surfaces for Non-Point Source Pollution Modeling. *Proceedings of 2000 American Society of Photogrammetry and Remote Sensing (ASPRS) Annual Conference,* Washington, D.C., May 22–26; American Society of Photogrammetry and Remote Sensing, Bethesda, Maryland.

Stefanov, W. L.; Ramsey, M. S.; Christensen, P. R. (2001) Monitoring Urban Land Cover Change: An Expert System Approach to Land Cover Classification of Semiarid to Arid Urban Centers. *Remote Sensing Environ.,* **77** (2), 173–185.

Stenstrom, M. K.; Silverman, G. S.; Bursztynsky, T. A. (1984) Oil and Grease in Urban Stormwaters. *J. Environ. Eng. ASCE,* **110** (1), 58–72.

Stenstrom, M. K.; Strecker, E. (1993) *Assessment of Storm Drain Sources of Contaminants to Santa Monica Bay*, Vol. I, Annual Pollutants Loadings to Santa Monica Bay from Stormwater Runoff, UCLA-ENG-93-62, I, 1-248; University of California: Los Angeles, California.

Varis, O. (1998) A Belief Network Approach to Optimization and Parameter Estimation: Application to Resource and Environmental Management. *Artificial Intelligence,* **101** (1–2), 135–163.

Vaze, J.; Chiew, F. H. S. (2003) Comparative Evaluation of Urban Storm Water Quality Models. *Water Resources Res.,* **39** (10), 1280–1289.

Viessman, Jr., L. G. L.; Knapp, J. W. (1989) *Introduction to Hydrology.* Harper and Row Publishers, Inc.: New York.

Wong, K.; Strecker, E. W.; Stenstrom, M. K. (1997) A Geographic Information System to Estimate Stormwater Pollutant Mass Loadings. *J. Environ. Eng. ASCE,* **123,** 737–745.